A Space Object Detection Algorithm using Fourier Domain Likelihood Ratio Test

Maj. David J. Becker
Air Force Institute of Technology

Dr. Stephen Cain
Air Force Institute of Technology

ABSTRACT

Space object detection is of great importance in the highly dependent yet competitive and congested space domain. Detection algorithms employed play a crucial role in fulfilling the detection component in the situational awareness mission to detect, track, characterize and catalog unknown space objects. Many current space detection algorithms use a matched filter or a spatial correlator to make a detection decision at a single pixel point of a spatial image based on the assumption that the data follows a Gaussian distribution. This paper explores the potential for detection performance advantages when operating in the Fourier domain of long exposure images of small and/or dim space objects from ground based telescopes. A binary hypothesis test is developed based on the joint probability distribution function of the image under the hypothesis that an object is present and under the hypothesis that the image only contains background noise. The detection algorithm tests each pixel point of the Fourier transformed images to make the determination if an object is present based on the criteria threshold found in the likelihood ratio test. Using simulated data, the performance of the Fourier domain detection algorithm is compared to the current algorithm used in space situational awareness applications to evaluate its value.

1. INTRODUCTION

Safe and dependable operations in the space domain are vital to the national security interests of the United States (U.S.). According to the 2011 U.S. National Security Space Strategy, "space is vital to U.S. national security and our ability to understand emerging threats, project power globally, conduct operations, support diplomatic efforts, and enable global economic viability" [1]. In order to preserve continued space operations, the 2010 U.S. National Space Policy called out the need to fund and develop technologies to "detect, identify, and attribute actions in space that are contrary to responsible use and the long-term sustainability of the space environment" [2]. Additionally, the National Space Policy stated the need to "pursue capabilities to detect, track, catalog, and characterize near-Earth objects to reduce the risk of harm to humans from an unexpected impact on our planet and to identify potentially resource-rich planetary objects".

The detection of either asteroids or man-made objects or debris represent similar challenges to those looking to detect, track and catalog unknown space objects. Due to their small size when viewed from a ground based telescope, these objects are likely to be similar to an unresolvable point source on the image captured by the charge-coupled device (CCD). This research is focused on improving the capability to detect dim and small space objects such as satellites and space debris to improve space situational awareness (SSA) from data obtained with current ground based electro-optic systems. The ability to detect dim objects is greatly impacted by the performance of the detection algorithm used to filter the data and make a determination if an unknown space object is present in the noisy scene. This paper proposes an improvement upon current detection algorithms by developing a binary hypothesis test (BHT) based on a likelihood ratio test (LRT) of the real component of the Fourier transform of the data. The LRT makes a detection decision based on the expected statistics of the data when an object is present in the data and when the data contains only background light sources. The results of the Fourier LRT are compared to the performance of a spatial domain matched filter algorithm similar to the one used within the space community whose mission is asteroid and/or debris detection. Converting the data into the frequency domain provides the benefit of greater separation in the probability distribution functions (PDFs) of the data when an object is present compared to when an object is not present. This separation is realized using a covariance matrix which shows there is a level of covariance experienced between spatial frequencies that are not present in traditional spatial data.

In Section 2 of this paper a description of the models for the atmosphere, noise parameters used in this paper are explained. Section 3 contains an explanation of the matched filter approach used in many space object detection processes. Additionally, this section builds the statistical model along with parameters needed to build the Fourier

LRT. This section develops the joint PDF used in the LRT as well as a modified version of the Fourier LRT that is used in this paper. Section 4 shows results obtained using MATLAB simulated data with the two different algorithms. The results are shown utilizing a receiver operating characteristic (ROC) curve to illustrate the probability of detection (P_D) versus the probability of false alarm (P_{FA}) for the Fourier detector compared to the spatial matched filter. Section 5 concludes with a discussion of the results and additional future research.

2. SYSTEM MODELS

The principle operation of telescopes is to map the intensity of a scene in the object plane onto the imaging plane of the CCD detector of the optical system. Physically, this is a model of how the electromagnetic wave propagates through space from the object to the detector. To develop the detection process and simulate data, an accurate model for the atmospheric conditions and the optical image formed are essential to testing under different conditions.

2.1 Long Exposure Atmospheric Model

In many SSA ground based telescope systems, the integration time is significantly long enough that it operates in the long exposure regime. When operating at these exposure times, the long exposure point spread function (PSF) and optical transfer function (OTF) are used to model the average size and spatial frequency content of a point source object viewed through a telescope [3]. The long exposure OTF for a circular aperture telescope is defined as

$$H_L(f_x, f_y) = \exp\left[\left(\frac{\bar{\lambda} z \sqrt{{f_x}^2 + {f_y}^2}}{r_0}\right)^{5/3}\right]. \quad (1)$$

Where $\overline{\lambda}$ is the mean wavelength, z is the telescope focal length and f_x and f_x are spatial frequencies. The Fried atmospheric seeing parameter, r_0, is a measure of the quality of optical propagations through the atmosphere [4]. As defined in Eq. (2), the long exposure OTF can be converted into the spatial domain to obtain the long exposure PSF, $h(x, y)$.

$$h(x, y) = \Im^{-1}\{H_L(f_x, f_y)\} \quad (2)$$

It is the inherent nature of the atmosphere over time to average out and this is shown in the zero mean Gaussian distribution of the random Zernike coefficients modeling the turbulent atmosphere. Thus, the long exposure PSF averages the random phase fluctuations due to the atmosphere to produce a spatially large PSF. On average, a long exposure PSF will contain zero tilt and will be an even and symmetric function.

2.2 Noise Statistics

In any optical telescope system, there are numerous sources of noise that adversely affect the ability to detect dim objects. These include the discrete nature of photon counting noise, background light, read out noise, dark current and thermal noise. The systems deployed for SSA applications generally utilize advanced hardware that limits the primary concern to the Poisson distributed photon counting noise and assumes a Gaussian distributed noise for all other sources.

2.2.1 Photon Counting

Photon noise or shot noise is a result of the CCD array in the detector plane array. The CCD is a discrete device that counts the number of photons that arrive at each element of the array. The distribution of the photons is modeled as a Poisson process where photons arrive at random intervals with a mean number of photons,k, arriving over a set time interval. The probability of k photons, $P(k)$, being counted at each pixel spot is given by the Poisson probability mass function (PMF) shown in Eq. (3) [3]. Photon counting noise results in the same object imaged at two different instances of time to appear to have different intensities.

$$P(k) = \frac{\bar{k}^k e^{-k}}{k!} \text{ for } k = 1,2,3 \ldots \quad (3)$$

2.2.2 Background Light

Background noise is the result of any light or signal aside from the light propagating from the object that is measured by the detector. There are various sources of background noise and many are dependent on the situation, they include but are not limited to the sun, starlight and building or city lights reflecting off other surfaces and captured by the primary mirror of the telescope. The background light, B, can be estimated during data capture by moving to a nearby dark spot of the sky to calibrate the camera or can be accomplished during real time or post-processing by taking the median value of all N pixels in each dimension of the windowed data, $d(x, y)$.

$$B = median(d(x, y) \forall (x, y) \in [1, N]) \quad (4)$$

3. DETECTION ALGORITHMS

Space object detection algorithms currently utilize single and multiple spatial images obtained from ground based telescopes. Many SSA platforms use multiple frames in their processing chain, however they start with being able to detect on a single frame and use the multiple frames of follow-up data to confirm or reject the detection decision. This research in this paper is focused on improving the ability to detect a dim space object from a single frame of data so that detection can be passed on for further multi-frame analysis technique and follow-up. The detection processes sometimes includes some amount of pre-processing of the data to do task such as measure background, remove bad pixels or remove known objects using a celestial map.

The performance of the detection algorithm is defined by its ability to maintain an acceptable amount of false alarms while recording detections. The probability of detection, P_D, is the probability of correctly determining that an object is present at a given location whereas the probability of false alarm, P_{FA}, is the probability that the algorithm determines an object is present at the tested pixel location when there is no object truly present. The P_{FA} is usually set to an extremely low level that is acceptable to meet mission and resource constraints since there are potentially millions of pixels to test in a single frame and each detection requires follow-up analysis.

3.1 MATCHED FILTER

A matched filter or spatial correlation algorithm is utilized to achieve a desired probability of false alarm when searching for an unknown space object. This approach is commonly used in space detection applications due to its superior performance over a point detector and its relatively fast computing time [5]. The algorithm is based on correlating or matching the observed data with the expected PSF from a point source object to obtain a sufficient statistic. To perform the correlation with the captured image, the expected PSF must be known. Typically, knowledge of the PSF has been limited to the long exposure case were the shape and size of the PSF can be determined from measurable statistical parameters of the atmosphere and can be considered on average to be a known value as was shown in Eq. (1) and (2). The matched filter is described mathematically by Eq. (5) [6].

$$SNR_{MF} = \frac{\sum_x \sum_y (d(x - x_0, y - y_0) - B) h(x, y)}{\sigma} \quad (5)$$

Where $d(x, y)$ is the data from a single image frame of data obtained from the telescope. The current pixel location being tested is denoted by (x_0, y_0). N is the size of the window region of interest in pixels, h is the known long exposure PSF and B is the median background noise level in photons. The standard deviation of the noise in the image, σ, is estimated for each frame of data using the following equation:

$$\sigma = \frac{1}{N^2} \sqrt{\sum_x \sum_y (d(x - x_0, y - y_0) - B)^2} \quad (6)$$

Under Gaussian noise assumptions, the SNR calculated in Eq. (5) is a zero mean, unit variance Gaussian random variable. Comparing this value to a threshold allows the operator to set the probability of false alarm at the desired rate. For example, if the threshold is set to 6, then the probability of false alarm or assigning a detection when no object is truly present would be approximately equal to 10^{-9}.

3.2 FOURIER LIKELIHOOD RATIO TEST

Unlike the matched filter described in the previous subsection, the algorithm proposed in this subsection operates based on a developed LRT of the data in the Fourier domain. A generic LRT takes a ratio of the PDFs of the data conditioned on each hypothesis. If this ratio is greater than 1, then the H_1 hypothesis is deemed true. Conversely, if the ratio is less than 1 then the H_0 ratio is true. The key to detection success in a LRT approach is correctly identifying the distribution along with accurate parameters needed to define that PDF.

The Fourier LRT in this paper is built using the statistics of the real component of the Fourier transform of the background subtracted data received by the optical system. The Fourier LRT, Λ, is defined using the joint conditional probabilities of the data under each hypothesis.

$$\Lambda = \frac{P\left(Re\{D_r(f_x,f_y)\}\forall(f_x,f_y)|H_1\right)}{P\left(Re\{D(f_x,f_y)\}\forall(f_x,f_y)|H_0\right)} \gtrless_{H_0}^{H_1} 1. \tag{7}$$

Where the background removed real component of the Fourier domain data, $D_r(f_x,f_y)$, is defined as shown in Eq. (8) as the Fourier transform of the data minus the background, $d'(x,y)$.

$$\begin{aligned} D_r(f_x,f_y) = Re\{D(f_x,f_y)\} &\triangleq Re\{\Im\{d'(x,y)\}\} \\ &= Re\left\{\frac{1}{N}\sum_x\sum_y d'(x,y)e^{-j\frac{2\pi}{N}(xf_x+yf_y)}\right\} \\ &= \frac{1}{N}\sum_x\sum_y d'(x,y)\cos\left(\frac{2\pi}{N}(xf_x+yf_y)\right) \\ &= \frac{1}{N}\sum_x\sum_y (d(x,y)-B)\cos\left(\frac{2\pi}{N}(xf_x+yf_y)\right) \end{aligned} \tag{8}$$

Similar to the random phasor sum calculations accomplished by Goodman in [3], for a large *N*, the real component of the random variable will be approximately Gaussian distributed due to the central limit theorem. Thus, in order to define the Fourier LRT, the mean and variance of the conditional data is needed along with a covariance matrix to build a joint PDF.

Previous work has been completed to analytically derive the mean and variance of the conditional data along with the covariance matrix to build the Fourier LRT. This paper is focused on using simulated data to establish a sample mean, variance and covariance matrix which will then be used to build the Fourier LRT. Therefore, the steps in deriving the analytical solution to these terms will not be explained in this paper but the results summarized in the following subsections.

3.2.1 Null Hypothesis (H_0) Distribution Statistics

Under the H_0 hypothesis, it is assumed that the data doesn't contain an object. Thus, the received data is dominated by background light which follows a Poisson distributed with a mean of *B* as shown in Eq (9). It is assumed that the background level, *B*, is known based on estimated from the data or other sensors in the optical system. The background subtracted data, $d'(x,y)$, would then have an expected value of zero.

$$\mathrm{E}[d(x,y)|H_0] = B. \tag{9}$$

$$\mathrm{E}[d'(x,y)|H_0]=\mathrm{E}[d(x,y)-B|H_0]=0 \tag{10}$$

Using the results from Eq. (10), the mean of the real component of the background removed Fourier transformed data under H_0 hypothesis, μ_0, is found to be zero.

$$\begin{aligned}\mu_0 &= \mathrm{E}\left[D_r(f_x,f_y)|H_0\right] \\ &= \mathrm{E}\left[\frac{1}{N}\sum_x\sum_y (d'(x,y)|H_0)\cos\left(\frac{2\pi}{N}(xf_x+yf_y)\right)\right] \\ &= 0\end{aligned} \tag{11}$$

With zero mean, the variance of this component, ${\sigma_0}^2$, is found to related to the background. This is expected since the data is assumed to be dominated by Poisson distributed background noise.

$$\begin{aligned}{\sigma_0}^2 &= \mathrm{E}\left[\left(D_r(f_x,f_y)|H_0\right)^2\right]-{\mu_0}^2 \\ &= \mathrm{E}\left[\left(\frac{1}{N}\sum_x\sum_y (d'(x,y)|H_0)\cos\left(\frac{2\pi}{N}(xf_x+yf_y)\right)\right)^2\right] \\ &= \frac{B}{2}\end{aligned} \tag{12}$$

An analytical derivation of the covariance matrix under the H_0 hypothesis, Σ_0, is defined using the standard form for covariance given in Eq. (13). The covariance matrix can be solved for using the values previously derived in this subsection along with the Poisson moment theorem for simplifying the expression.

$$\begin{aligned}\Sigma_0 &= \mathrm{E}\left[D_r(f_{x_1},f_{y_1})D_r(f_{x_2},f_{y_2})\right]-{\mu_0}^2 \\ &= \frac{B}{2}\delta(f_{x_1}-f_{x_2},f_{y_1}-f_{y_2})\end{aligned} \tag{13}$$

The covariance matrix is found to be an identity matrix scaled by the variance. This result is as expected and implies that there is on average zero correlation between spatial frequencies when no object is present.

3.2.2 Alternate Hypothesis (H_1) Distribution Statistics

Under the H_1 hypothesis, it is assumed that the data contains an object along with background noise. The assumption is made that the object is unresolvable and can be modeled as an intensity scaled point source represented by the PSF, $h(x,y)$. Thus, the mean of the spatial data can be modeled as

$$\mathrm{E}[d(x,y)|H_1]=\theta h(x,y)+B. \tag{14}$$

The mean of the background subtracted data, $d'(x,y)$, is then defined as

$$\mathrm{E}[d'(x,y)|H_1]=\mathrm{E}[d(x,y)-B|H_1]=\theta h(x,y). \tag{15}$$

Using the results from Eq. (15), the mean of the real component of the background removed Fourier transformed data under H_1 hypothesis, μ_1, is found in Eq. (16).

$$\begin{aligned}\mu_1 &= \mathrm{E}\left[D_r(f_x,f_y)|H_1\right] \\ &= \mathrm{E}\left[\frac{1}{N}\sum_x\sum_y (d'(x,y)|H_1)\cos\left(\frac{2\pi}{N}(xf_x+yf_y)\right)\right] \\ &= \theta H(f_x,f_y)\end{aligned} \tag{16}$$

Where $H(f_x,f_y)$ is defined as the Fourier transform of the PSF or OTF as given in Eq. (1).

The variance under the H_1 hypothesis, ${\sigma_1}^2$, is not as straight forward to calculate as the null hypothesis due to the added complications from the non-zero mean. The analytical solution to the variance is given in the equation below.

$$\begin{aligned}{\sigma_1}^2 &= \mathrm{E}\left[\left(D_r(f_x,f_y)|H_1\right)^2\right] - {\mu_1}^2 \\ &= \mathrm{E}\left[\left(\frac{1}{N}\sum_x\sum_y (d'(x,y)|H_1)\cos\left(\frac{2\pi}{N}(xf_x+yf_y)\right)\right)^2\right] - \left(\theta H(f_x,f_y)\right)^2 \\ &= \frac{B}{2} + \frac{\theta}{2N^2} + \frac{\theta}{N}H(2f_x,2f_y) + \frac{B}{2N}\delta(f_x,f_y)\end{aligned} \tag{17}$$

Under dim object scenarios, the $B/2$ term, which was equal to the variance found in the H_0 hypothesis, is going to dominate. The additional terms in ${\sigma_1}^2$ will always be positive and will result in the H_1 data containing a larger variance. The additive variance will vary based on the intensity of the target and the frequency being examined. Shown in Fig. 1 is a plot of the difference in the variance in a single dimension using the data simulated under the first scenario in Section 4 of this paper. Due to the Dirac function and the OTF in Eq. (17), the variance will be largest when evaluated at the DC or zero frequency. When looking at spatial frequencies away from zero, the variance will quickly begin to approach the variance of the H_0 hypothesis.

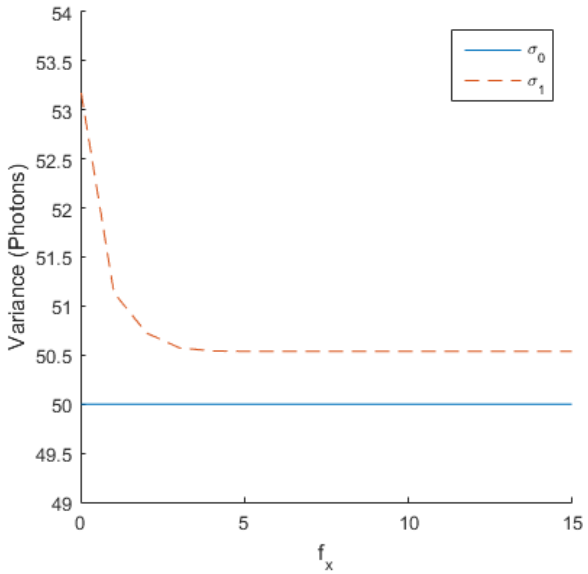

Fig. 1: Analytical variance under each hypothesis for B=100, θ = 1100, N=32.

Similar to the previous subsection, an analytical derivation of the covariance matrix under the H_1 hypothesis, Σ_1, is defined using the standard form for covariance similar to that given in Eq. (13) except the mean and data is conditioned on H_1. The covariance matrix is given in Eq. (18). Like above, the covariance contains a non-zero mean that complicates the analytical derivation.

$$\begin{aligned}\Sigma_1 &= E\left[D_r(f_{x_1},f_{y_1})D_r(f_{x_2},f_{y_2})\right] - {\mu_1}^2 \\ &= \frac{B}{2}\delta(f_{x_1}-f_{x_2},f_{y_1}-f_{y_2}) + \frac{\theta}{2N}H(f_{x_1}-f_{x_2},f_{y_1}-f_{y_2}) + \frac{\theta}{2N}H(f_{x_1}+,f_{y_1}+f_{y_2})\end{aligned} \tag{18}$$

The derived covariance matrix is very similar to Σ_0 but not exactly the same. Like the derived variance, there are additive terms based on the OTF, target intensity and window size that will add non-zero elements to the covariance matrix. This implies that when an object is present in the scene there is some amount of correlation among frequencies. It is this correlation that the Fourier LRT will exploit to improve the detection performance.

3.2.3 Likelihood Ratio Test

Using the mean, variance, and covariance matrix derived in the previous subsections, the Fourier LRT can be built by returning to Eq. (7) and substituting the PDF for a multivariate Gaussian random variable.

$$\Lambda = \frac{(2\pi)^{-\frac{1}{2}N}|\Sigma_1|^{-\frac{1}{2}}e^{-\frac{1}{2}(D_r-\mu_1)^T{\Sigma_1}^{-1}(D_r-\mu_1)}}{(2\pi)^{-\frac{1}{2}N}|\Sigma_0|^{-\frac{1}{2}}e^{-\frac{1}{2}(D_r-\mu_0)^T{\Sigma_0}^{-1}(D_r-\mu_0)}} \gtrless_{H_0}^{H_1} 1. \tag{19}$$

The data, D_r, is a $1xN^2$ vector, the ${\Sigma_0}^{-1}$ and ${\Sigma_1}^{-1}$ terms are size $N^2 \times N^2$ and represent the inverse of the covariance matrices, $|\Sigma_1|$ and $|\Sigma_0|$ are the determinant of each covariance matrix. The means, μ_0 and μ_1, are $1xN^2$ vectors representing the mean of the conditional data at each spatial frequency pair f_x, f_y.

Cancelling terms and taking the natural log simplifies the Fourier LRT to the following expression. Due to taking the natural log of both sides the threshold is zero and the greater than or less than designations have been flipped.

$$-(D_r-\mu_1)^T{\Sigma_1}^{-1}(D_r-\mu_1) + (D_r-\mu_0)^T{\Sigma_0}^{-1}(D_r-\mu_0) \lessgtr_{H_0}^{H_1} 0 \tag{20}$$

This expression can be further simplified down to the expression shown in Eq. (21) by expanding out the matrix multiplications, substituting the means and further combining terms. The right side of the equation has been replaced with τ to represent the threshold since specific threshold values are not examined in this paper as a ROC curve is used to evaluate performance.

$$-{D_r}^T{\Sigma_1}^{-1}D_r + {D_r}^T{\Sigma_0}^{-1}D_r + 2(\theta H)^T{\Sigma_1}^{-1}D_r \lessgtr_{H_0}^{H_1} (\theta H)^T{\Sigma_1}^{-1}(\theta H) \equiv \tau \tag{21}$$

The Fourier LRT in this form represents some challenges that must be solved before it could be implemented using measured data. The first issue is the need to know the target intensity, θ, if an object was in the image. In a detection scenario this value will not be known and estimating it from the data will be difficult since the algorithm would have to estimate the intensity when an object wasn't in the scene as well. A similar challenge exists in creating each of the covariance matrix since both also have dependence on the target intensity.

The Fourier LRT investigated further in this paper is going to take components of the complete Fourier LRT derived above to simplify the test and remove the dependency on θ. This modified approach is shown in Eq. (22). The modified Fourier LRT utilizes the covariance matrix along with the Fourier transformed data to build a LRT and make a detection decision. It can be shown that the second term of the Fourier LRT is simply a representation of the spatial correlator in the frequency domain. Thus, this LRT is taking the data derived by the spatial correlator using a Fourier transform and including additional information that is available via the covariance of the data among different frequencies in the Fourier domain.

$$H^T{\Sigma_1}^{-1}D_r + H^T{\Sigma_0}^{-1}D_r \lessgtr_{H_0}^{H_1} \tau \tag{22}$$

4. SIMULATED DATA

Dim space object data was simulated in MATLAB to test the performance of the Fourier LRT algorithm compared to the matched filter algorithm. The MATLAB simulation allows access to accurately distributed and realistic looking data while removing unknowns in the scenarios. Under the H_1 hypothesis, the intensity of the object can be varied to test the algorithm at various SNR levels and data under the H_0 hypothesis can be simulated by setting the intensity to zero. The simulation will develop data with accurate long exposure PSF statistics and utilizing built in Poisson random variable functions to simulate the statistics of the background noise.

The simulation was set up for two different scenarios using the parameters shown in Table 1. The first scenario represents a D/r_0 ratio of 5 and the second represents slightly better atmospheric conditions with a D/r_0 of 3. The intensity level was adjusted in each scenario to simulate a signal-to-noise ratio (SNR) 6 object which has a P_D of 0.5 when the P_{FA} is at 10^{-9} using the spatial correlator.

Table 1. Parameters used to simulate data under two different scenarios.

Parameter	Scenario 1	Scenario 2
Aperture diameter, D (m)	0.25	0.25
Atmospheric Seeing, r_0 (m)	0.05	0.08
Target intensity, θ (photons)	1050	700
Background, B (photons)	100	100
Window size, N (pixels)	32	32
Frames of data for each hypothesis	100	100

Examples of the simulated data are shown in Fig. 2 which illustrates one frame of simulated data obtained from the optical system under each of the hypothesis for the first scenario. Fig. 3 shows the associate long exposure PSF that was simulated to create the long exposure data under the H_1 hypothesis that was shown in Fig. 2. The long exposure PSF was created by averaging 100 correlated short exposure PSFs generated using an approach developed by Putnam [7]. A single instance of the background removed Fourier transformed data for each hypothesis is shown in Fig. 4.

The covariance matrix used by the Fourier LRT was calculated from the data sample set. This is not the ideal scenario since it would prohibit real time processing of data but this technique could be utilized to build a covariance matrix based on the entire set of data in a post-processing detection algorithm.

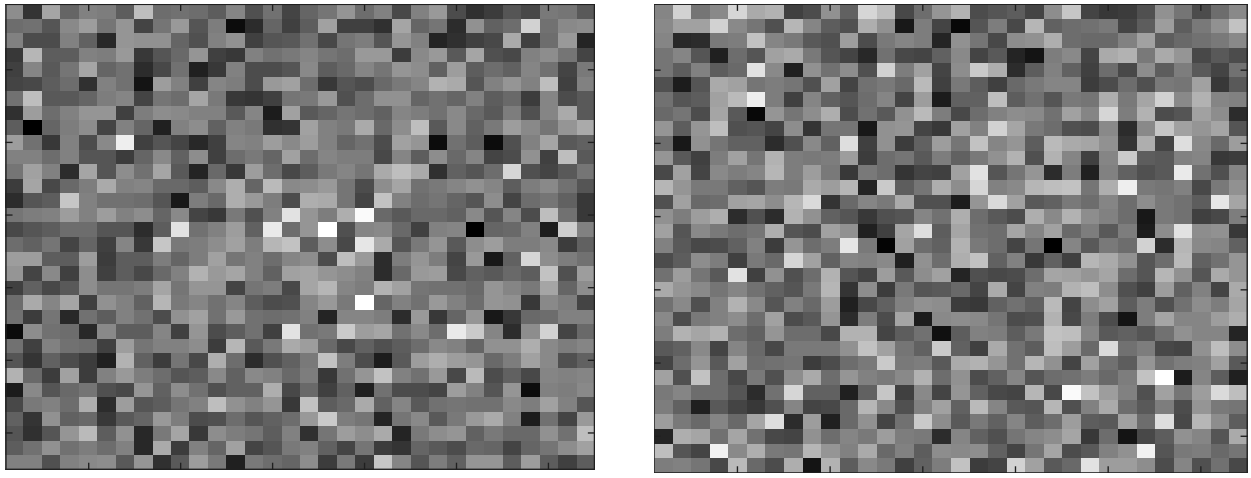

Fig. 2: An example of simulated H_1 data (left) and H_0 data (right) under the first scenario.

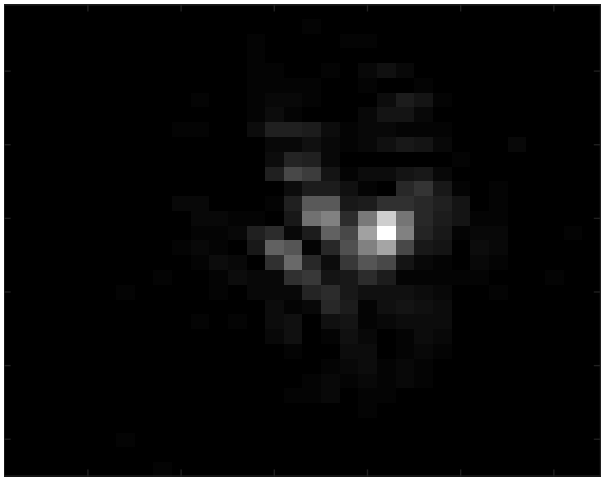

Fig. 3: Long exposure PSF used to generate the single instance of H_1 data shown in Fig. 2.

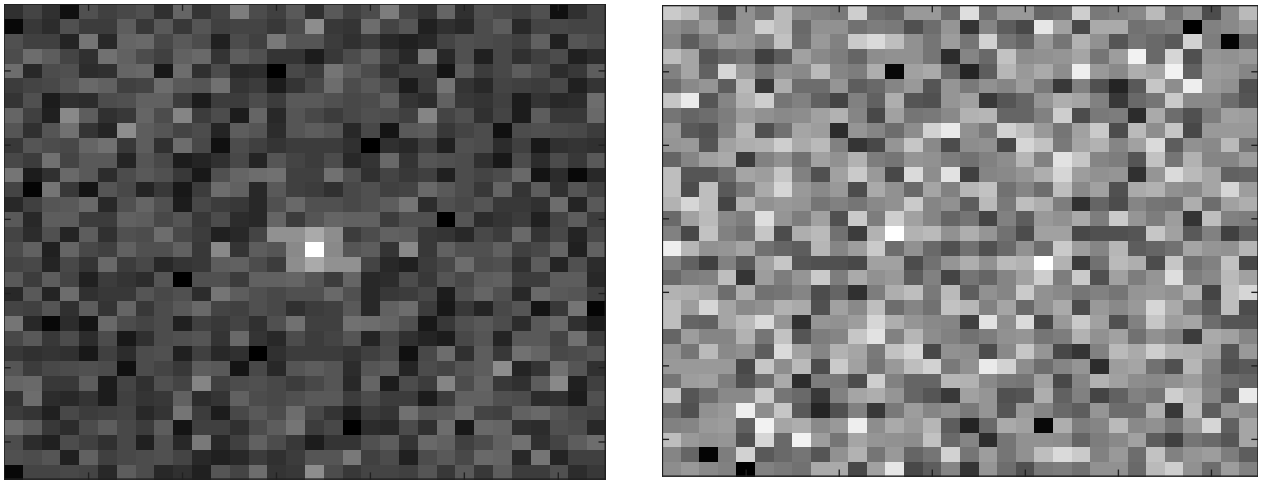

Fig. 4: Real component of the background removed Fourier transformed data. H_1 (left). H_0 (right).

5. RESULTS

The simulated data was used to evaluate the performance of the Fourier LRT against the spatial correlator with a ROC curve. The use of a ROC curve allows the performance to be evaluated without setting a specific threshold value. This showcases the performance of the algorithms at difference detection and false alarm rates. The ROC curve is generated by calculating the P_D and P_{FA} for a range of threshold values.

The ROC curve for each scenario is shown in Fig. 5. Under the first scenario a 18% increase in the P_D at a P_{FA} of 10^{-9} is accomplished by the Fourier LRT. Under the second scenario, the Fourier LRT achieved a 22% increase in P_D at a P_{FA} of 10^{-9} over the matched filter approach.

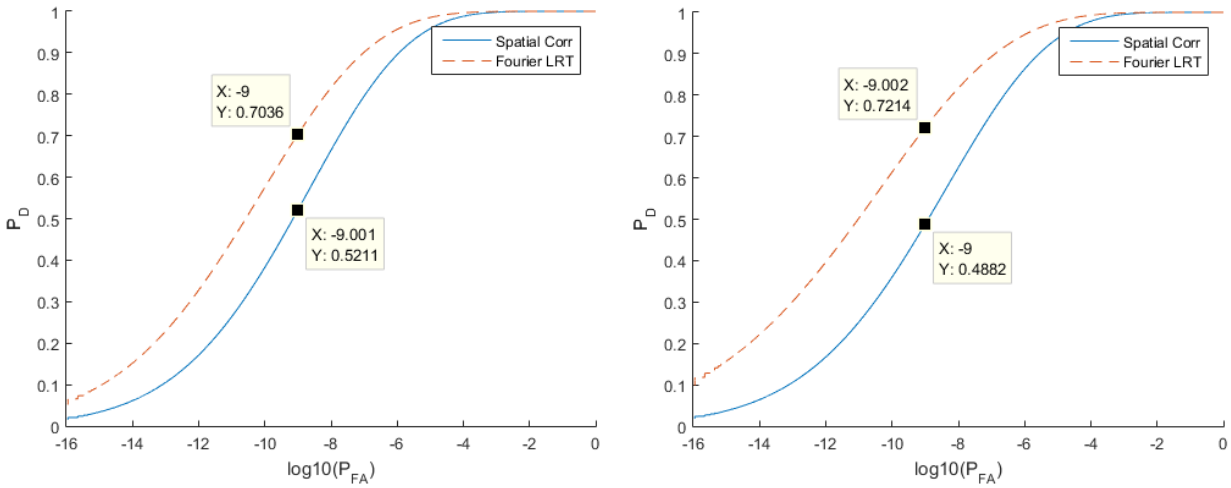

Fig. 5: ROC curve for the matched filter and Fourier LRT methods. Scenario 1, $D/r_0 = 5$ (left). Scenario 2, $D/r_0 = 3$ (right).

6. CONCLUSIONS

The results show that when using long exposure data, the Fourier LRT achieves a significant increase in the detection probability at realistic false alarm rates using the modified Fourier LRT compared to the matched filter approach. Both techniques assume that the background level is known along with knowing the atmospheric seeing conditions. The modified Fourier LRT approach used in this paper didn't depend on knowing the target intensity but did assume the covariance matrix could be calculated from the data when an object was present. This requires the algorithm to operate in a post-processing format and to potentially collect additional data knowing an object was present to generate the covariance matrix.

Further research is needed to implement the full Fourier LRT and to develop a solution based on having no prior information on the target intensity in the LRT or in the covariance matrix. This further research will determine if processing long exposure SSA data in the Fourier domain has an advantage of the traditional spatial data approach.

7. REFERENCES

[1] US Department of Defense and Office of the Director of National Defense, "National Security Space Strategy Unclassified Summary," p. 14, 2011.

[2] Office of the President of the United States of America, "National Space Policy of the United States of America," *United States Gov.*, p. 18, 2010.

[3] J. W. Goodman, *Statistical Optics*. New York: John Wiley & Sons, Inc., 2000.

[4] D. L. Fried, "Optical Resolution Through a Randomly Inhomogeneous Medium for Very Long and Very Short Exposures," *J. Opt. Soc. Am.*, vol. 56, no. 10, p. 1372, 1966.

[5] J. C. Zingarelli, "ENHANCING GROUND BASED TELESCOPE PERFORMANCE WITH IMAGE PROCESSING," Air Force Institute of Technology, 2013.

[6] T. Hardy, "OPTICAL THEORY IMPROVEMENTS TO SPACE DOMAIN AWARENESS," Air Force Institute of Technology, 2016.

[7] I. Putnam, "Atmospheric Impact on Long Pulse Laser Detection and Ranging (LADAR) Systems," Air Force Institute of Technology, 2013.